High-Saturation-Current Modified Uni-Traveling-Carrier Photodiode With Cliff Layer

Zhi Li, Huapu Pan, Hao Chen, Andreas Beling, and Joe C. Campbell, *Fellow, IEEE*

***Abstract*—We demonstrate two modified uni-traveling carrier photodiode (MUTC) structures that incorporate a charge or "cliff" layer to attain high-saturation-current. MUTC1 achieved responsivity of 0.82 A/W and 134 mA saturation current at −6-V and 20 GHz. The MUTC2 structure, which has higher doping density in the cliff layer and thinner absorption region, exhibited a higher saturation current of 144 mA (at −5-V) and an improved 3 dB bandwidth of 24 GHz; however, the responsivity was reduced to 0.69 A/W. For MUTC2, a high-saturation-current × bandwidth product of 3456 GHz·mA has been achieved. An intermodulation distortion figure of merit, IP3, > 39 dBm at 20 GHz was observed for both MUTC structures.**

***Index Terms*—Photodetectors, photodiodes.**

I. Introduction

HIGH-SPEED analog optical links are attractive for microwave applications due to their ability to achieve low loss and high bandwidth and to resist electromagnetic interference [1]. As the optical-to-electrical converter in these links, it is advantageous for photodiodes to operate at very high photocurrent levels and, thus, high radio frequency (RF) output powers [2]. A primary factor that limits the saturation power of a photodiode is the carrier screening of the internal electric field, which is referred to as the space-charge effect. Uni-traveling-carrier (UTC) photodiodes [3] have been developed to enhance high-power performance while also achieving high speed and good linearity characteristics, since only high-drift-speed electrons are employed as active carriers in the drift/collection region. A UTC photodiode with a non-uniformly doped collector exhibited a bandwidth of 20 GHz, 120 mA average current, and responsivity of 0.55 A/W [4]. Shi *et al.* [5] reported a near-ballistic evanescently coupled waveguide UTC photodiode that achieved 32 mA at 40 GHz with responsivity of 1.14 A/W. A modified UTC photodiode [6] showed saturation current of 260 mA at 5 GHz and RF power of 29 dBm; the bandwidth was 7 GHz. Chtioui *et al.* [7] reported a UTC structure with a high responsivity of 0.83 A/W that achieved 24 GHz bandwidth and 80 mA saturation current measured at 10 GHz. A back-illuminated modified uni-traveling carrier (MUTC) photodiode attained saturation current of 110 mA, bandwidth of 17 GHz, and 0.75 A/W responsivity [8].

In this paper, we describe two charge-compensated modified uni-traveling-carrier (CC-MUTC) photodiode structures that will be referred to in the following as MUTC1 and MUTC2. These photodiodes advantageously employ a cliff layer [9] to achieve higher operating power than previously reported MUTC photodiodes [8]. The benefit of the cliff layer is to provide higher electric field in the depleted InGaAs absorber region, which enables higher current before space-charge induces saturation. Responsivity of 0.82 A/W was observed with an anti-reflection coating for MUTC1 photodiode. The 3 dB bandwidths of 34-μm and 28-μm-diameter devices were 20 GHz and 23 GHz with saturation currents of 134 mA (−6-V bias) and 102 mA (−5-V bias), respectively. Compared to the MUTC1 structure, MUTC2 has a thinner undepleted p-type absorber in order to achieve higher bandwidth, however, at the cost of lower responsivity (0.69 A/W). A second modification is higher doping in the cliff layer for higher saturation current. The 3 dB bandwidths of 34-μm and 28-μm-diameter MUTC2 photodiodes were 24 GHz and 32 GHz with saturation currents of 144 mA (−5-V bias) and 110 mA (−5-V bias), respectively. High output power of 22.7 dBm was realized at 24 GHz for the 34-μm-diameter MUTC2, which corresponds to a saturation-current/bandwidth product of 3456 GHz·mA.

II. Device Design and Fabrication

The MUTC1 structure was grown on semi-insulating double-side-polished InP substrates by metal-organic chemical vapor deposition. A schematic cross section is shown in Fig. 1. The epitaxial growth began sequentially with 200-nm-thick n^+ InP, 20 nm n^+ $In_{0.53}Ga_{0.47}As$, and 900 nm n^+ InP layers. A 100 nm n-type InP layer with a doping concentration of 1×10^{18} cm^{-3} was then grown to reduce Si diffusion into the following 900-nm lightly doped InP drift layer. Following the InP drift layer are three transition layers, a 50 nm InP cliff layer and two 15 nm lightly doped InGaAsP layers. The $In_{0.53}Ga_{0.47}As$ absorbing region consists of a 150-nm lightly doped n^- layer that is depleted when the device is biased for operation and four undepleted, step-graded p^+ layers. The

Manuscript received November 28, 2009; revised January 26, 2010 and February 26, 2010. Current version published May 28, 2010. This work was supported by Defense Advanced Research Projects Agency and the Naval Research Laboratory.

Z. Li, H. Pan, and H. Chen are with the Department of Electrical and Computer Engineering, University of Virginia, Charlottesville, VA 22904 USA (e-mail: zl4s@virginia.edu; hp5n@virginia.edu; hc3r@virginia.edu).

A. Beling and J. C. Campbell are with the University of Virginia, Charlottesville, VA 22904 USA (e-mail: beling@u2t.de; jccuva@virginia.edu).

Color versions of one or more of the figures in this paper are available online at http://ieeexplore.ieee.org.

Digital Object Identifier 10.1109/JQE.2010.2046140

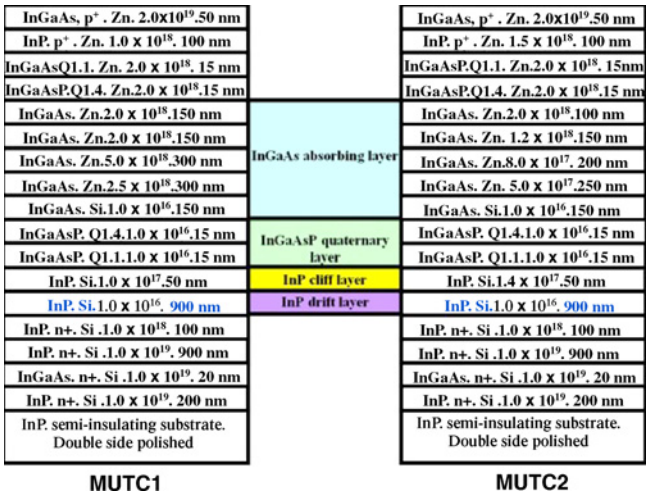

Fig. 1. InGaAs-InP MUTC1 and MUTC2 photodiode structure.

two top layers are a 100 nm p^+ InP electron blocking layer and a 50 nm p^+ $In_{0.53}Ga_{0.47}As$ contact layer. The function of the two 15 nm InGaAsP quaternary layers is to "smooth" the abrupt conduction band barrier at the InGaAs-InP heterojunction interface. In the p-type $In_{0.53}Ga_{0.47}As$ absorbing region, the doping was graded in four steps (2.5×10^{17} cm^{-3}, 5.0×10^{17} cm^{-3}, 1.0×10^{18} cm^{-3}, and 2.0×10^{18} cm^{-3}) in order to create a quasi-electric field that assists electron transport. In the depletion region, the 900-nm InP layer, the 150-nm depleted $In_{0.53}Ga_{0.47}As$ absorbing layer, and the two InGaAsP transition layers were n-type-doped to $\sim 10^{16}$ cm^{-3} for the purpose of charge compensation [10]. Compared to the previously reported MUTC design reported in [8], the total thickness of the $In_{0.53}Ga_{0.47}As$ absorbing layer was increased from 850 nm to 1100 nm to increase the responsivity. The thickness of the charge-compensated InP collector layer was increased from 605 nm to 900 nm to reduce the capacitance and thus increase the resistance-capacitance component of the bandwidth. The InP cliff layer, which is a thin InP layer n-doped to 1×10^{17} cm^{-3}, was added between the charge-compensated $In_{0.53}Ga_{0.47}As$ and InP layers to reduce the deleterious effect of space-charge at high photocurrent levels [11].

The thickness of the $In_{0.53}Ga_{0.47}As$ absorbing layer in MUTC2 was decreased to 850 nm to enhance the transit-time limited bandwidth. The p-type $In_{0.53}Ga_{0.47}As$ was graded in four steps (5.0×10^{17} cm^{-3}, 8.0×10^{17} cm^{-3}, 1.2×10^{18} cm^{-3}, and 2.0×10^{18} cm^{-3}). The doping density of the InP cliff layer was raised to $1.4 \times 10^{17} cm^{-3}$ to enhance saturation current.

Back-illuminated mesa structures were fabricated by inductive coupled plasma etching. Microwave contact pads and air-bridge connections to the top p-contact layer were fabricated for high-speed measurements. Finally, a 230-nm-thick SiO_2 anti-reflection layer was deposited on the back of the wafer. The fiber-coupled external quantum efficiencies for MUTC1 and MUTC2 at 1550-nm wavelength were 66% and 55%, respectively. The devices were mounted on a thermo-electric heat sink for testing.

III. Saturation Current Enhancement by Cliff Layer

Saturation occurs when the space-charge-induced electric field reduces the carrier velocity below the saturation velocity, which in turn degrades the bandwidth. Previously, non-uniform doping methods have been proposed to reduce the space-charge effect. A dual-depletion region photodiode [12] employs three-section-charge compensation in the dual-depletion region to enhance the saturation current and the UTC photodiode in [4] uses a half-doped collector to mitigate the space-charge effect. For the MUTC structure, the electron space-charge in the depleted collector, together with the electron and hole space-charge in the depleted absorber ultimately, causes the field intensity to collapse in the depleted absorber under high current operation. The reduced electric field impedes electron transport across the band discontinuity at the InGaAs/InP heterojunction interface, which reduces the carrier velocity. One approach to enhance the saturation current is to increase the field in the depleted absorber region. In order to improve the noise and speed performance of separate-absorption-charge-and-multiplication avalanche photodiodes, a charge layer is employed to maintain a high electric field in the multiplication region [13]. A similar charge or "cliff" layer has been incorporated into the CC-MUTC design to enhance the electric field intensity in the depleted absorber and, thus, mitigate the space-charge-induced field collapse in the depleted InGaAs absorption layer.

For the same absorber and collector parameters as MUTC1, cliff layers with different thicknesses and doping densities were simulated in APSYS. Fig. 2(a) and (b) shows the current responses under DC illumination for cliff layer thicknesses from 10 nm to 130 nm and doping densities in the range 5×10^{16} cm^{-3} to 2×10^{17} cm^{-3}. For each curve, the photocurrent density initially exhibits a linear increase with illumination power density. The inflection points, where the slope decreases with increasing optical power, occur because the reduced field at the heterojunction interfaces allows the conduction band barriers to block electron injection into the InP collector. The decrease of slope suggests a reduced responsivity under high power illumination. The emergence of junction barriers also reduces the carrier velocity due to the fact that the trapped electrons traverse the barrier via thermal emission. This causes a reduction in the bandwidth and thus saturation. Since the reduced responsivity and bandwidth degradation are closely related through the space-charge-induced electric field, it can be inferred that the inflection points in Fig. 2(a) and (b) provide an indirect indicator of saturation current. These simulations show that a high thickness/doping density product results in higher saturation current up to the point where the field becomes too low in the InP collector. Based on the simulations, a moderate thickness of 50 nm was selected for both structures. The nominal cliff layer doping densities for MUTC1 and MUTC2 were $1 \times 10^{17}/cm^3$ and $1.4 \times 10^{17}/cm^3$, respectively.

Fig. 3 shows the simulated photocurrent response of MUTC1. A responsivity of 0.83 A/W is extracted from the slope of the linear part, which agrees very well with the measured 0.82 A/W responsivity. An average current density

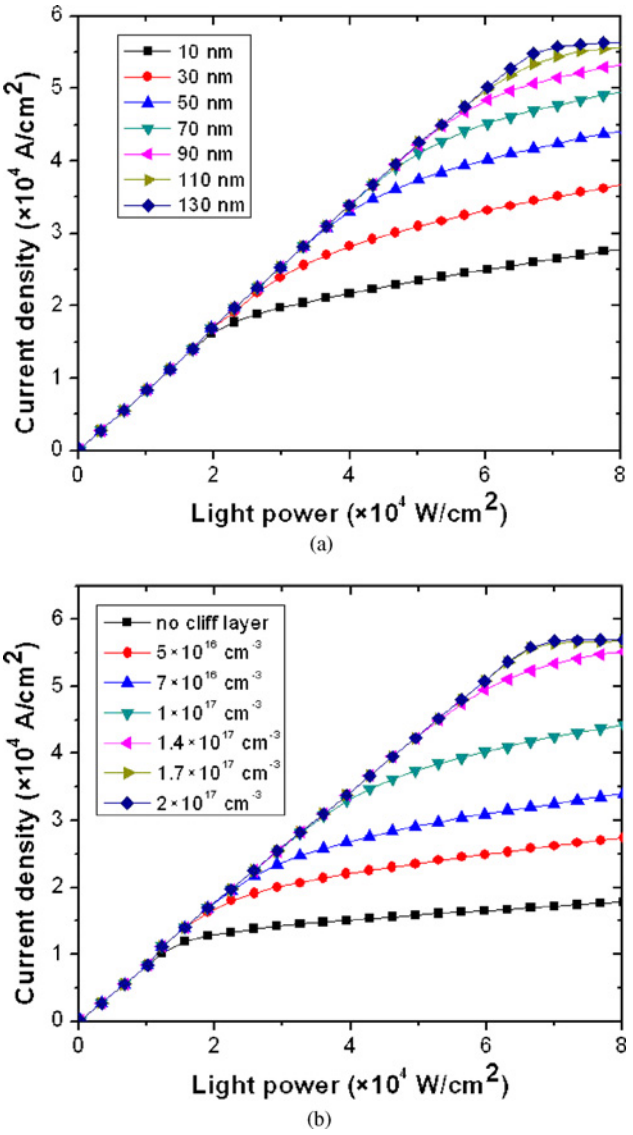

Fig. 2. (a) Simulated photocurrent response under DC illumination at 6-V reverse bias for different cliff layer thicknesses. The doping density is $1\times10^{17}/\text{cm}^3$. (b) Simulated photocurrent response under DC illumination at 6-V reverse bias for different cliff layer doping densities. The thickness is 50 nm.

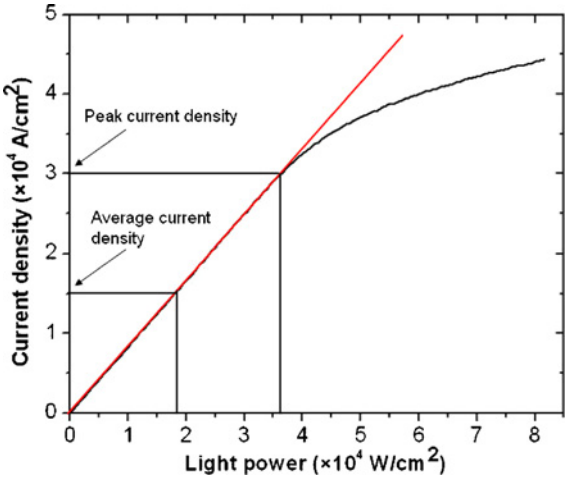

Fig. 3. Simulated photocurrent response under DC illumination at 6-V reverse bias for the CC-MUTC epi-structure.

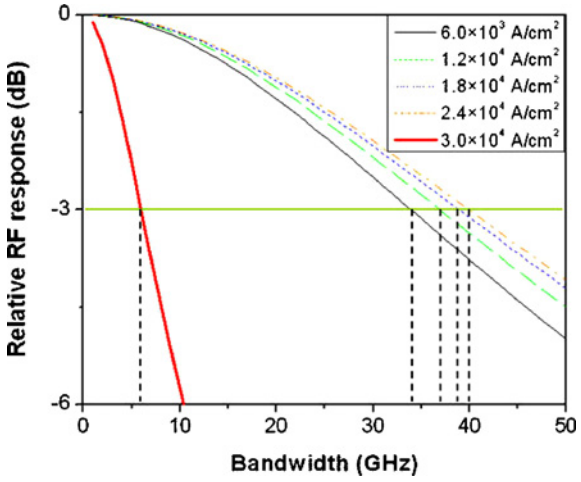

Fig. 4. Simulated small-signal relative RF response for different average photocurrent density at 6-V reverse bias.

of 1.5×10^4 A/cm^2 was measured for a 34 μm device at 6-V reverse bias at the -1 dB compression point. Assuming 100% modulation depth, the peak current density is 3×10^4 A/cm^2, which is near the inflection point in Fig. 3. An increase of the average photocurrent beyond 1.5×10^4 A/cm^2 will take the device further into saturation.

Simulation of the transit-time-limited small-signal response in Fig. 4 is consistent with this conclusion. At an average current density of 3×10^4 A/cm^2, which is also the peak current density marked in Fig. 3, the small-signal 3 dB bandwidth drops significantly to only 6 GHz compared with 40 GHz at 2.4×10^4 A/cm^2 photocurrent density. It follows that increasing the average photocurrent density beyond 1.5×10^4 A/cm^2 exacerbates saturation and that the model is an effective predictor of the saturation current density.

IV. Bandwidth and Compression Measurement

The frequency response and saturation current were measured using large-signal modulation. A 100% modulated heterodyne optical signal was generated by mixing two ~1550 nm distributed-feedback lasers with slightly different wavelength. By sweeping the frequency of the signal, which was achieved by changing the temperature and thus the wavelength of one laser, the bandwidths of the photodiodes of various sizes were measured. Prior to measurements of the saturation current and third-order intermodulation distortions (IMD3) the lensed fiber was retracted slightly to ensure uniform illumination. The lens was located at a position where the responsivity decreased to approximately half its maximum value. This resulted in stable, repeatable measurements.

Fig. 5(a) and (b) shows the relative RF power versus frequency of 34-μm-diameter MUTC1 and MUTC2 photodiodes measured at a photocurrent of 90 mA, respectively. The 3 dB bandwidth of the 34-μm-diameter MUTC2 device shows a 4 GHz improvement compared to the MUTC1 device of the same diameter owing to its thinner undepleted InGaAs absorber.

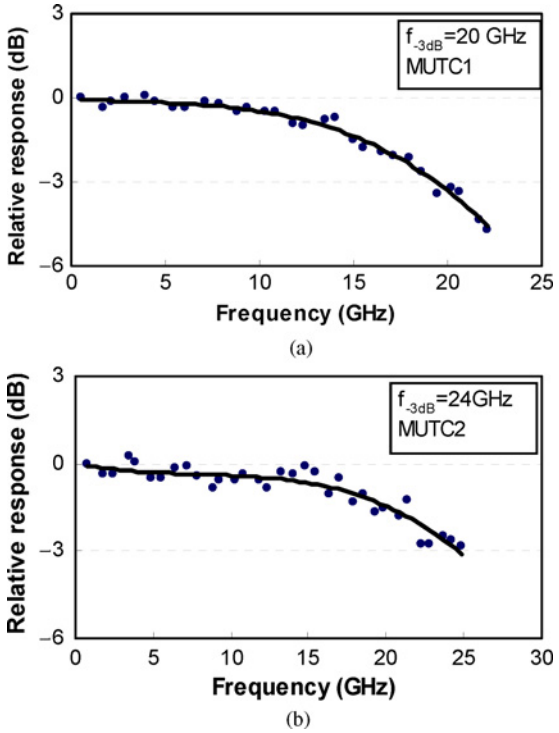

Fig. 5. (a) Frequency response of 34 μm MUTC1 device at a photocurrent of 90 mA. (b) Frequency response of 34 μm MUTC2 device at a photocurrent of 90 mA.

The saturation current was measured at the 3 dB bandwidth frequency. The photodiodes were mounted on a thermo-electric cooler with a surface temperature of 10 °C. Fig. 6 shows the RF output power versus average photocurrent for a 34-μm-diameter MUTC2 at 24 GHz for 4-V, 5-V, and 6-V reverse biases. Since these measurements were made at the 3 dB bandwidth, a 3 dB difference between the "ideal" curve and the measured RF output power would be expected. However, the difference is >3 dB for current values < 90 mA. This suggests that the -3 dB bandwidth of 24 GHz is reached only at high current. Similar to other UTC-like photodiodes, the measured RF power experiences a super-linear increase with the photocurrent before saturation occurs. This is caused by the bandwidth improvement due to the self-induced electric field in the graded-doped InGaAs absorber [14]. The enhancement behavior is shown in the inset of Fig. 6. A maximum output power of +23.1 dBm was realized at 140 mA, signal frequency of 24 GHz, and 6-V reverse bias. When tested at room temperature without a thermo-electric cooler, the device died at 110 mA without exhibiting saturation.

Compression, which is defined as the difference between measured RF power and ideal linear power in dB, was measured versus photocurrent at different reverse biases for devices having diameters of 28, 34, 40, and 56 μm. Fig. 7 shows the compression of a 34-mm-diameter MUTC2 photodiode at 24 GHz versus photocurrent. The Compression is normalized to be 0 dB at low photocurrent. The marked "1 dB" in Fig. 7 illustrates our working definition of the -1 dB saturation point. In contrast to the definition in [4], which defines the -1-dB saturation current as the photocurrent at which the compression drops to -1 dB, in this paper the -1 dB

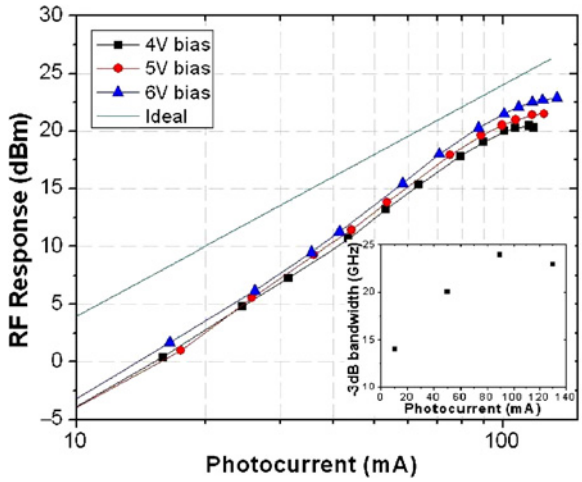

Fig. 6. RF output power of a 34-μm-diameter MUTC2 device at 24 GHz versus photocurrent at reverse biases of 4-V, 5-V, and 6-V. The inset shows the -3 dB bandwidth for different photocurrent values (10, 50, 90, and 130 mA).

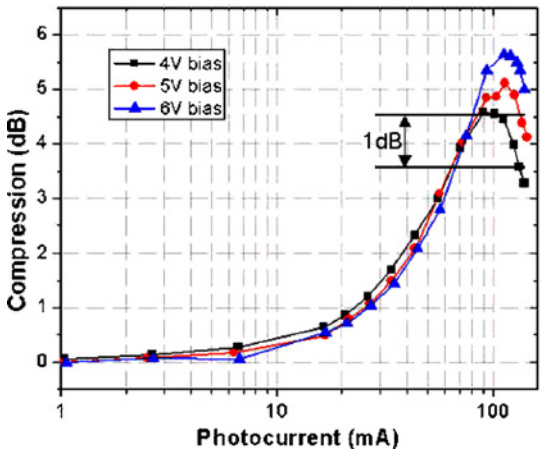

Fig. 7. Compression of a 34-μm-diameter MUTC2 device at 24 GHz at 4, 5, and 6-V reverse biases. The -1 dB compression level is marked to show saturation currents.

saturation current is defined as the photocurrent at which the RF response decreases by 1 dB from its peak. We think this more stringent definition is more relevant since saturation effects are observed when the compression starts to drop from its peak. We note that the measured saturation current by this definition is smaller than the value that would be obtained using the definition in [4]. Based on our definition of saturation current, the maximum saturation current-bandwidth products for 34 μm and 28 μm MUTC2 photodiodes are 3456 and 3264 GHz·mA, respectively.

Tables I and II summarize the bandwidth, saturation current and output RF power of MUTC1 and MUTC2, respectively, for different device diameters and bias voltages. "Failure" refers to catastrophic failure prior to saturation. Compared with the results reported in [8], the bandwidth of the 34 μm MUTC2 has increased from 17 GHz to 24 GHz and the saturation current has increased from 110 mA to 144 mA. With a higher doping density in the cliff layer, the MUTC2 structure tends to achieve higher saturation current than the MUTC1 structure under the same conditions, by suppressing the space-charge

TABLE I

BANDWIDTH, SATURATION CURRENT, AND RF OUTPUT POWER OF 28-, 34-, 40-, AND 56-μM-DIAMETER MUTC1 DEVICES UNDER 5, 6, AND 7-V REVERSE BIAS

Diameter (μm)	3 dB Bandwidth (GHz)	I_s (mA) and [P_{out} (dBm)] at 4-V	I_s (mA) and [P_{out} (dBm)] at 5-V	I_s (mA) and [P_{out} (dBm)] at 6-V
28	23	95 [18.9]	102 [20.6]	Failure at 110 mA
34	20	118 [20.3]	125 [21.5]	134 [22.9]
40	15	139 [21.9]	149 [23.2]	Failure at 155 mA [23.9 at 147 mA]
56	8	140 [22.1]	162 [24]	174 [25.1]

I_s and P_{out} are the saturation current and RF output power, respectively.

TABLE II

BANDWIDTH, SATURATION CURRENT, AND RF OUTPUT POWER OF 28-, 34-, 40-, AND 56-μM-DIAMETER MUTC2 DEVICES UNDER 5, 6, AND 7-V REVERSE BIAS

Diameter (μm)	3 dB Bandwidth (GHz)	I_s (mA) and [P_{out} (dBm)] at 4-V	I_s (mA) and [P_{out} (dBm)] at 5-V	I_s (mA) and [P_{out} (dBm)] at 6-V
28	32	103 [19.2]	110 [21]	Failure at 112 mA
34	24	132 [21]	144 [22.7]	Failure at 145 mA [23.1 at 140 mA]
40	18	135 [21.9]	146 [23.7]	Failure at 152 mA
56	11	152 [22.8]	168 [24.4]	190 [26]

I_s and P_{out} are the saturation current and RF output power, respectively.

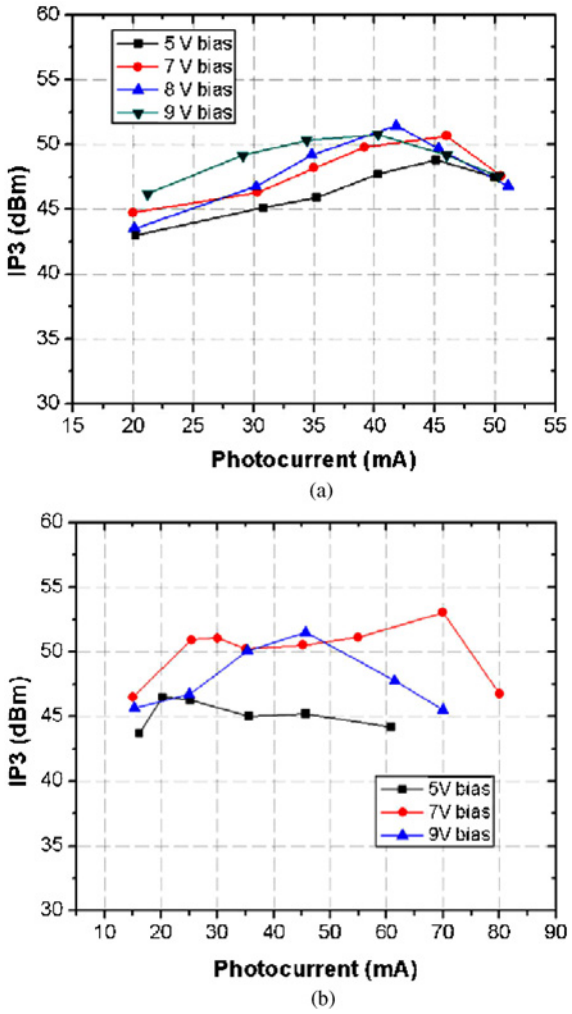

Fig. 8. (a) Measured IP3 of a 40-μm-diameter MUTC1 device versus photocurrent at 5, 7, 8, and 9-V reverse biases at 320 MHz. (b) Measured IP3 of a 40-μm-diameter MUTC2 device versus photocurrent at 5-V, 7-V, and 9-V reverse biases at 320 MHz.

effect. Based on the simulation in Fig. 2(b), the MUTC2 structure should have 50% improvement in saturation current relative to the MUTC1 structure. However, the actual improvement was much lower as a result of several negative factors, such as the reduction in bias-voltage that is caused by the voltage swing in the load resistance and the gradual device failure due to thermal runaway.

V. MEASUREMENT OF INTERMODULATION DISTORTION

When considering the nonlinearity in photodiodes, the IMD3 are of particular interest because their frequencies may be close to the fundamental modulation frequencies. Conventionally, the power of the fundamental signals and the IMD3 are measured using a standard two-tone setup. The two-tone, third-order output intercept point (OIP3) is defined as OIP3 = $P_f + \Delta P/2$ with $\Delta P = P_f - P_{\mathrm{IMD3}}$, assuming that the power of the IMD3 increases with a slope of 3 [15]. However, the OIP3 measured by the conventional two-tone setup could be influenced by the harmonics produced by the optical modulators, which would introduce inaccuracies. A three-tone setup, which is less sensitive to nonlinearities in the response of the optical modulators, has been proposed in [16]. This measurement technique was employed for the IMD3 measurements reported here. Different from the conventional two-tone measurements, where the output RF signals at the fundamental frequencies f_1, f_2 and the IMD3 at $(2 \times f_2 - f_1)$ and $(2 \times f_1 - f_2)$ are measured, the three-tone technique measures the output RF signals at the fundamental frequencies f_1, f_2, f_3 and the IMD3 at $(f_1 + f_2 - f_3)$, $(f_2 + f_3 - f_1)$, $(f_3 + f_1 - f_2)$. When comparing results obtained by the three-tone technique with those obtained with the conventional two-tone setup, a factor of 3 dB needs to be added to the measured three-tone OIP3 as described in [16].

The OIP3 of 40 mm MUTC1 and MUTC2 devices versus photocurrent were measured at 320 MHz at different reverse biases and the results are plotted in Fig. 8(a) and (b). The highest OIP3 of 53 dBm was achieved at 70-mA photocurrent and 7-V reverse bias for the MUTC2 structure.

Fig. 9 shows the frequency dependence of OIP3 for MUTC1 at a photocurrent of 40 mA and a reverse bias of 8-V and MUTC2 at a photocurrent of 70 mA and a reverse bias of 7-V, respectively. The voltage and current for each device are those that maximize OIP3. The OIP3 up to 20 GHz remains above 40 dBm for the MUTC1 structure and above

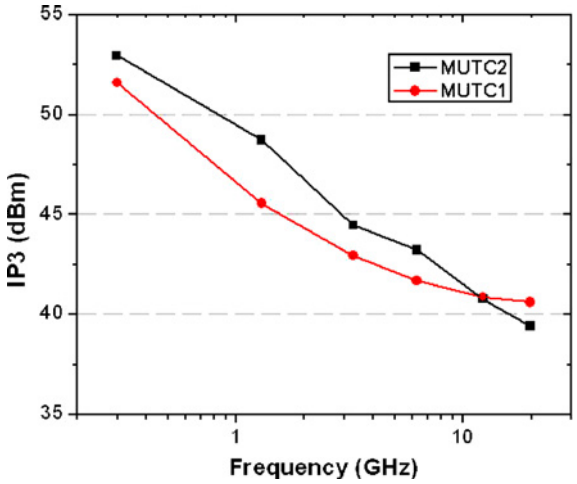

Fig. 9. Measured IP3 of a 40-μm-diameter MUTC1 device in dependence of frequency at a photocurrent of 40 mA and a reverse bias of 8-V and a 40-μm-diameter MUTC2 device in dependence of frequency at a photocurrent of 70 mA and a reverse bias of 7-V.

39 dBm for the MUTC2. We note that OIP3 of MUTC2 is approximately 1 dB higher than MUTC1 when the frequency is less than 10 GHz. Such an improvement may be due to the fact that MUTC2 has a slightly thinner depleted absorber at the same reverse bias because it has a higher doping density in the p-type-doped InGaAs layer adjacent to the lightly n-type-doped InGaAs absorber. That helps MUTC2 achieve a reduced voltage-dependent relative responsivity compared with that of MUTC1 [17] and therefore a higher OIP3 at low frequency. Those results compare favorably with the UTC photodiode that attained an OIP3 of 35 dBm at 20 GHz and 40 mA [18] or the CC-MUTC photodiode that achieved an OIP3 of 36 dBm at 20 GHz and 50 mA [19]. An InGaAs/InP partially depleted absorber photodiode with a highly doped absorber was reported to have an OIP3 of 39 dBm at 20 GHz. However, the OIP3 at lower frequency was only ~38 dBm [20].

VI. Conclusion

In conclusion, two types of back-illuminated high-power modified uni-traveling carrier photodiodes with cliff layer structures have been demonstrated. The saturation current enhancement by cliff layer has been theoretically investigated and supported by the experimental data. A high-saturation-current×bandwidth product of 3456 GHz·mA has been achieved for the MUTC2 structure with a responsivity of 0.69 A/W. A high OIP3 of 53 dBm was achieved for the MUTC2 structure. OIP3 >39 dBm was measured up to 20 GHz for both structures.

References

[1] A. J. Seeds, "Microwave photonics," *IEEE Trans. Microw. Theory Tech.*, vol. 50, no. 3, pp. 877–887, Mar. 2002.

[2] T. Nagatsuma, "Photonic measurement technologies for high-speed electronics," *Meas. Sci. Tech.*, vol. 13, no. 11, pp. 1655–1663, Nov. 2002.

[3] T. Ishibashi and N. Shimizu, "Uni-traveling-carrier photodiodes," in *Proc. Ultrafast Electron. Optoelectron. Conf.*, Incline Village, NV, 1997, pp. 83–87.

[4] M. Chtioui, A. Enard, D. Carpentier, S. Bernard, B. Rousseau, F. Lelarge, F. Pommereau, and M. Achouche, "High-performance uni-traveling-carrier photodiodes with a new collector design," *IEEE Photonics Technol. Lett.*, vol. 20, no. 13, pp. 1163–1165, Jul. 2008.

[5] J.-W. Shi, Y.-S. Wu, C.-Y. Wu, P.-H. Chiu, and C.-C. Hong, "High-speed, high-responsivity, and high-power performance of near-ballistic uni-traveling-carrier photodiode at 1.55 mm wavelength," *IEEE Photon. Technol. Lett.*, vol. 17, no. 9, pp. 1929–1931, Sep. 2005.

[6] S. Itakura, K. Sakai, T. Nagatsuka, T. Akiyama, Y. Hirano, E. Ishimura, M. Nakaji, and T. Aoyagi, "High-current backside-illuminated InGaAs/InP p-i-n photodiode," in *Proc. Int. Topical Meeting Microwave Photon. (MWP)*, Oct. 2009, pp. 1–4.

[7] M. Chtioui, D. Carpentier, S. Bernard, B. Rousseau, F. Lelarge, F. Pommereau, C. Jany, A. Enard, and M. Achouche, "Thick absorption layer uni-traveling-carrier photodiodes with high responsivity, high speed, and high saturation power," *IEEE Photon. Technol. Lett.*, vol. 21, no. 7, pp. 429–431, Apr. 2009.

[8] X. Wang, N. Duan, H. Chen, and J. C. Campbell, "InGaAs-InP photodiodes with high responsivity and high saturation power," *IEEE Photon. Technol. Lett.*, vol. 19, no. 16, pp. 1272–1274, Aug. 2007.

[9] N. Shimizu, N. Watanabe, T. Furuta, and T. Ishibashi, "Improved response of uni-traveling-carrier photodiodes by carrier injection," *Jpn. J. Appl. Phys.*, vol 37, pp. 1424–1426, Mar. 1998.

[10] K. J. Williams and R. D. Esman, "Design considerations for high-current photodetectors," *J. Lightw. Technol.*, vol. 17, pp. 1443–1454, Aug. 1999.

[11] H. Pan, A. Beling, H. Chen, and J. C. Campbell, "Characterization and optimization of high-power InGaAs/InP photodiodes," *Opt. Quantum Electron.*, vol. 40, no. 1, pp. 41–46, 2008.

[12] K. J. Williams, "Comparisons between dual-depletion-region and uni-traveling-carrier p-i-n photodetectors," *IEE Proc.-Optoelectron.*, vol. 149, no. 4, pp. 131–137, Aug. 2002.

[13] H. Nie, K. A. Anselm, C. Hu, S. S. Murtaza, B. G. Streetman, and J. C. Campbell, "High-speed resonant-cavity separate absorption and multiplication avalanche photodiodes with 130 GHz gain-bandwidth product," *Appl. Phys. Lett*, vol. 70, pp. 161–163, Jan. 1997.

[14] H. Ito, S. Kodama, Y. Muramoto, T. Furuta, T. Nagatsuma, and T. Ishibashi, "High-speed and high-output InP-InGaAs unitraveling-carrier photodiodes," *IEEE J. Sel. Topics Quantum Electron.*, vol. 10, no. 4, pp. 709–727, Jul. 2004.

[15] K. J. Williams, L. T. Nichols, and R. D. Esman, "Photodetector nonlinearity limitation on a high-dynamic range 3 GHz fiber optic link," *J. Lightw. Technol.*, vol. 16, no. 2, pp. 192–199, Feb. 1998.

[16] A. Ramaswamy, J. Klamkin, N. Nunoya, L. A. Johansson, L. A. Coldren, and J. E. Bowers, "Three-tone characterization of high-linearity waveguide uni-traveling-carrier photodiodes," in *Proc. 21st Annu. Meeting IEEE Lasers Electro-Opt. Soc. (LEOS)*, 2008, pp. 286–287.

[17] H. Pan, A. Beling, and J. C. Campbell, "High-linearity uni-traveling-carrier photodiodes," *IEEE Photon. Technol. Lett.*, vol. 21, no. 24, pp. 1855–1857, Dec. 2009.

[18] M. Chtioui, A. Enard, D. Carpentier, S. Bernard, B. Rousseau, F. Lelarge, F. Pommereau, and M. Achouche, "High-power high-linearity uni-traveling-carrier photodiodes for analog photonic links," *IEEE Photon. Technol. Lett.*, vol. 20, no. 3, pp. 202–204, Feb. 2008.

[19] A. Beling, H. Pan, C. Hao, and J. C. Campbell, "Measurement and modeling of a high-linearity modified uni-traveling carrier photodiode," *IEEE Photon. Technol. Lett.*, vol. 20, no. 14, pp. 1219–1221, Jul. 2008.

[20] H. Pan, A. Beling, H. Chen, and J. C. Campbell, "The frequency behavior of the intermodulation distortions of modified uni-traveling carrier photodiodes based on modulated voltage measurements," *IEEE J. Quantum Electron.*, vol. 45, no. 3, pp. 273–277, Mar. 2009.

Zhi Li was born in Changle, Fujian, China, in 1985. He received the B.S. degree in optical engineering from Zhejiang University, Zhejiang, China, in 2007. He is currently working toward the Ph.D. degree in microelectronics from the Department of Electrical and Computer Engineering, University of Virginia, Charlottesville.

He is conducting research on high-power, high-speed photodetectors.

Huapu Pan was born in Chengdu, China, in 1984. He received the B.S. degree in physics from Peking University, Beijing, China, in 2006. He is currently working toward the Ph.D. degree in microelectronics from the Department of Electrical Engineering, University of Virginia, Charlottesville.

His current research is focused on high-power, high linearity photodetectors.

Hao Chen was born in Fuzhou, China, in 1983. He received the B.S. degree in microelectronics from Fudan University, Shanghai, China, in 2005 and received the M.S. degree in 2009. He is currently working toward the Ph.D. degree from the Department of Electrical Engineering, University of Virginia, Charlottesville.

His current research interests include high-power, high linearity photodetectors, and analog optical links.

Andreas Beling was born in Bonn, Germany, in 1973. He received the Dipl.-Phys. degree (M.S.) in physics from the University of Bonn, Bonn, Germany, in 2000, and the Dr.-Ing. degree (Ph.D.) in electrical engineering from Technical University Berlin, Berlin, Germany, in 2006.

In 2000, he was a Research Assistant with the Max Planck Institute for Radio Astronomy. From 2001 to 2006, he was a Staff Scientist with the Photonics Division, Heinrich-Hertz-Institut für Nachrichtentechnik (HHI). With HHI, he was engaged in the design and characterization of high-speed optoelectronic circuits. In 2007, he joined Prof. Joe C. Campbell's Group, University of Virginia, Charlottesville, as a Research Associate. His current research interests include high-power high-speed photodetectors and microwave photonics.

Joe C. Campbell (S'73–M'74–SM'88–F'90) received the B.S. degree in physics from the University of Texas, Austin, in 1969, and the M.S. and Ph.D. degrees in physics from the University of Illinois at Urbana-Champaign, Champaign, in 1971 and 1973, respectively.

From 1974 to 1976, he was Member of Technical Staff with Texas Instruments, Dallas, where he worked on integrated optics. In 1976, he was Member of Technical Staff with AT&T Bell Laboratories, Crawford Hill Laboratory, Holmdel, NJ, where he worked on a variety of optoelectronic devices, including semiconductor lasers, optical modulators, waveguide switches, photonic integrated circuits, and photodetectors with emphasis on high-speed avalanche photodiodes for high-bit-rate lightwave systems. In 1989, he joined the faculty of the University of Texas, Austin, as a Professor of Electrical and Computer Engineering and Cockrell Family Regents Chair in Engineering. In 2006, he became a Member of Faculty with the University of Virginia, Charlottesville, as the Lucian Carr, III Chair of Electrical Engineering and Applied Science. Currently, he is actively involved in single-photon-counting avalanche photodiodes, Si-based optoelectronics, high-speed, low-noise avalanche photodiodes, ultraviolet photodetectors, and quantum-dot infrared imaging. To date, he has coauthored six book chapters, 320 articles for refereed technical journals, and more than 200 conference presentations. His current research has focused on the optoelectronic components that are used to generate, modulate, and detect the optical signals.

Dr. Campbell is a Member of the National Academy of Engineering, a Fellow of the Optical Society of America, and a Fellow of the American Physical Society.